Gelatin Binding to the ^{6}F1^{1}F2^{2}F2 Fragment of Fibronectin Is Independent of Module−Module Interactions†

Amanda Pagett, Iain D. Campbell,* and Andrew R. Pickford

Department of Biochemistry, University of Oxford, South Parks Road, Oxford OX1 3QU, U.K.

Received May 20, 2005; Revised Manuscript Received September 6, 2005

ABSTRACT: Fibronectin, a large modular protein, interacts with many other proteins in the extracellular matrix and on the cell surface. It has previously been shown that interactions between noncontiguous modules exist in the collagen binding region. It is shown here that the interaction between the sixth type I module (^{6}F1) and the second type II module (^{2}F2) can be disrupted by mutation of a residue in the intermodule interface of the ^{6}F1^{1}F2^{2}F2 fragment. The perturbation of the interface and the binding of collagen-derived peptides to individual modules were assessed by high-resolution nuclear magnetic resonance (NMR) spectroscopy. Cooperativity between the modules in binding ligand was assessed by analytical gelatin affinity chromatography of the mutant and wild-type proteins. Differential scanning calorimetry (DSC) was used to probe the influence of the interface on module stability. It is shown that while the ^{6}F1−^{2}F2 interface confers significant thermal stability to the ^{2}F2 module, it has little effect on gelatin binding activity of the ^{6}F1^{1}F2^{2}F2 fragment.

Fibronectin is a large glycoprotein that plays a structural and organizational role in mammalian tissues. It is primarily made up of three different types of repeating protein modules of less than 100 amino acids, here called F1, F2, and F3 (*29*). Extracellular matrix fibronectin is secreted by a variety of cells and is actively organized into a detergent-insoluble, multimeric fibrillar network (*1*−*4*). Fibronectin also modulates cell migration in processes such as embryogenesis, wound repair (*5*, *6*), anchorage-dependent cell growth, and proliferation (*2*, *5*, *7*, *8*).

Fibronectin has been shown to bind collagen types I, II, III, IV, and V in vitro (*9*−*11*); it appears to bind to collagen type I with an axial periodicity similar to that of collagen type I fibrils, suggesting that there is one binding site per triple helix (*10*). The cyanogen bromide fragment from the α1 collagen chain, α1(I)-CB7, is the best characterized fibronectin binding fragment (*12*), and the region from residue 772 to residue 785, which has a low proline/hydroxyproline content, has been implicated in fibronectin binding (*9*). In vitro, fibronectin binds to denatured collagen (gelatin) with a higher affinity than native collagen (*9*, *13*). The 42 kDa proteolytic fragment of fibronectin, encompassing modules ^{6}F1^{1}F2^{2}F2^{7}F1^{8}F1^{9}F1 (the nomenclature ^{n}F*X* means the *n*th type *X* module), retains most of fibronectin's collagen/gelatin binding activity (*14*−*16*). F2 modules are involved in the collagen binding activities of many proteins (*17*, *18*), but studies of numerous fragments and deletion mutants of the gelatin binding domain show that almost all of the modules in the 42 kDa fragment are important (*19*). This suggests that cooperativity between multiple binding sites on the modular structure is important.

The nuclear magnetic resonance (NMR)[1] solution structure of a fragment of the gelatin binding domain, ^{6}F1^{1}F2^{2}F2, has been published. This structure shows a well-defined interaction between the noncontiguous modules ^{6}F1 and ^{2}F2 (*20*). The physiological role of this interface is, however, unclear, and this paper examines this interaction between ^{6}F1 and ^{2}F2 and its role in gelatin binding affinity and protein stability. It is shown here that mutation of alanine 114, a residue in the center of the ^{6}F1−^{2}F2 interface, to aspartate disrupts the interface without causing significant perturbations to the structure of the ^{2}F2 module. Differential scanning calorimetry (DSC) is used to show that the ^{6}F2−^{2}F2 interface contributes significantly to ^{2}F2 stability. Perhaps surprisingly, disruption of the ^{6}F2−^{2}F2 interface has very little effect on the gelatin binding properties of the ^{6}F1^{1}F2^{2}F2 construct as shown by gelatin affinity chromatography.

MATERIALS AND METHODS

Protein Production. Specific mutations in fibronectin fragments ^{6}F1^{1}F2^{2}F2(A114D) and ^{1}F2^{2}F2(A114D) were created using overlap extension PCR. The mutant fragments were cloned into the yeast expression vector pPIC9K for production in *Pichia pastoris*. Transformation was performed using Invitrogen protocols (www.invitrogen.com). Protein degradation was significantly greater for all of the A114 mutants compared to the wild-type proteins as assessed by SDS−PAGE. Despite the apparent proteolysis, ^{6}F1^{1}F2^{2}F2(A114D) and ^{1}F2^{2}F2(A114D) produced enough protein to enable their analysis. Expression of unlabeled and uniformly ^{15}N-labeled ([u-^{15}N]) proteins was carried out in a 1 L fermenter (Electrolab Ltd., Tewkesbury, U.K.) following

† The authors thank the Wellcome Trust and BBSRC for financial support.

* Corresponding author. E-mail: iain.campbell@bioch.ox.ac.uk. Telephone: +44 1865 275346. Fax: +44 1865 275253.

[1] Abbreviations: DSC, differential scanning calorimetry; RP-HPLC, reverse-phase high-pressure liquid chromatography; NMR, nuclear magnetic resonance.

10.1021/bi050937i CCC: $30.25
Published on Web 10/14/2005

published protocols (*21*). The proteins were purified from fermentation supernatant by a combination of cation-exchange chromatography, gelatin affinity chromatography, and reverse-phase high-pressure liquid chromatography (RP-HPLC) (*20*). Prior to the RP-HPLC step, the high-mannose oligosaccharide attached to N125 in the ^{2}F2 module was trimmed using the enzyme Endo H_f, leaving a single N125-linked *N*-acetylglucosamine residue. The protein products were analyzed by electrospray mass spectrometry and N-terminal sequencing.

NMR Data Acquisition. All NMR experiments were acquired on spectrometers operating at 600.1 or 750.1 MHz for ^{1}H. Samples were prepared by dissolving either [u-^{15}N]-^{1}F2^{2}F2(A114D), [u-^{15}N]^{6}F1^{1}F2^{2}F2(A114D), [u-^{15}N]^{6}F1^{1}F2-^{2}F2, or [u-^{15}N]^{1}F2^{2}F2 to a final concentration of 0.5−1.5 mM in 90% H_2O/10% D_2O or 99.9% D_2O with 40 mM potassium phosphate buffer and 0.02% (w/v) sodium azide and adjusting the pH to 4.5. The following spectra were recorded in H_2O: a three-dimensional (3D) gradient-enhanced [^{1}H−^{15}N]-TOCSY-HSQC with 46 ms mixing time (*22*) and a 3D gradient-enhanced [^{1}H−^{15}N]-NOESY-HSQC with 60 ms mixing time (*22*).

NMR Data Processing and Analysis. NMR data processing was performed using the FELIX 2.3 software package (Biosym Technologies Inc.) as previously described (*20*). Proton chemical shifts were referenced relative to the standard 1,4-dioxane at 3.743 ppm, with indirect referencing in the ^{15}N dimension using a ^{15}N/^{1}H frequency ratio of 0.101329118 (*23*). The program NMRView 5.0.3 (Merck and Co., Inc.) was used for spectral assignment. Initial assignment of the backbone NH and HN resonances at 25 °C and pH 4.5 of the ^{1}F2^{2}F2(A114D) and ^{6}F1^{1}F2^{2}F2(A114D) point mutants was achieved by comparison with previous assignments under the same conditions for the wild-type ^{6}F1^{1}F2, ^{1}F2^{2}F2, and ^{6}F1^{1}F2^{2}F2 fragments (*20*, *24*). Confirmation of these initial assignments was obtained using the 3D gradient-enhanced [^{1}H−^{15}N]-TOCSY-HSQC and [^{1}H−^{15}N]-NOESY-HSQC data sets.

Differential Scanning Calorimetry. Samples of proteins at 1.7 mg/mL were dialyzed overnight against 0.15 M NaCl and 10 mM Na-HEPES, pH 7.4. Aliquots (1 mL) of the sample and dialysis buffer were degassed for 15 min prior to loading the sample and reference cells of a Calorimetry Systems Nano III calorimeter. All scans were preceded by 10 min equilibration at the starting temperature. In order to ensure the absence of gas in the samples, initial scans from 5 to 20 °C (at 1 °C/min) were repeated until a reproducible baseline was achieved. Three scans per sample were performed from 5 to 90 °C and back to 5 °C (at 1 °C/min).

Gelatin Affinity Chromatography. Affinity chromatography was performed on an XK26/16 column (Amersham Pharmacia Biotech) packed with 20 mL of gelatin−Sepharose 4B (A.P.B.). Samples (200 μL) of the fibronectin fragments were loaded at 4 mL/min at a concentration of 50 μM in phosphate-buffered saline (PBS), pH 7.4, washed with an equal volume of PBS, pH 7.4, and eluted isocratically at room temperature. The absorbance of the eluent was monitored at 280 nm, and the degree of binding was determined from the buffer volume required for elution.

NMR-Monitored Gelatin Peptide Titrations. The dissociation affinity constants for gelatin binding to the individual modules in each fragment were determined by NMR-monitored titrations with the gelatin-like peptide GPA-GAOGTOGPQGIAG (supplied by Alta Bioscience), where O is 4-hydroxyproline. This peptide includes the collagenase cleavage site in the collagen α1(I) chain. For each 0.5 mM fibronectin fragment sample, a ^{1}H,^{15}N-HSQC spectrum was collected at pH 4.5 for 10 titration points in the range 0−10 mM peptide. The spectra were processed as described above.

The interaction of ligand with *m* independent binding sites on a protein can be described by

$$[\mathrm{L}]^{\mathrm{free}} = [\mathrm{L}]^{\mathrm{total}} - [\mathrm{P}]^{\mathrm{total}} \sum_{s=1}^{m} f_s \qquad (1)$$

where $[\mathrm{L}]^{\mathrm{free}}$ is the concentration of uncomplexed ligand, $[\mathrm{P}]^{\mathrm{total}}$ is the total protein concentration, and f_s is the fractional occupancy of ligand binding site *s*, which is given by

$$f_s = \frac{[\mathrm{L}]^{\mathrm{free}}}{K_{\mathrm{d}}^{s} + [\mathrm{L}]^{\mathrm{free}}} \qquad (2)$$

where K_{d}^{s} is the dissociation constant for site *s*. In the fast exchange regime, the fractional occupancy of each site may be estimated from the relative chemical shift changes of reporting resonances:

$$f_s = \frac{1}{n_s} \sum_{r=1}^{n_s} \frac{\Delta^{r,s}}{\Delta_{\infty}^{r,s}} \qquad (3)$$

where n_s is the number of resonances reporting on site *s*, $\Delta^{r,s}$ is the chemical shift change of resonance *r* from the ligand-free condition, and $\Delta_{\infty}^{r,s}$ is the chemical shift difference of this resonance between the ligand-free and ligand-saturated conditions. Therefore, by titrating the system to saturation and thus determining $\Delta_{\infty}^{r,s}$ for each reporting resonance, the K_{d} values can be determined by nonlinear least-squares fitting to the data. However, where binding is weak (e.g., with a $K_{\mathrm{d}} \gg 1$ μM) solubility limitations may prevent the determination of $\Delta_{\infty}^{r,s}$. Such is the case for this study. To overcome this, the K_{d} and $\Delta_{\infty}^{r,s}$ values were determined by an iterative Monte Carlo algorithm that minimized the χ^2 difference between the observed and back-calculated $\Delta^{r,s}$ values. Starting from initial estimations, the K_{d} and $\Delta_{\infty}^{r,s}$ were randomly increased or decreased by up to 10% in 1 million iterations. Only those changes that resulted in a reduction in χ^2 were accepted. Errors in the K_{d} and $\Delta_{\infty}^{r,s}$ were determined by incorporating random Gaussian errors (with a standard deviation of 0.005 ppm, the digital resolution of the HSQC spectra) into the experimental $\Delta^{r,s}$ values and repeating the fitting procedure 100 times.

RESULTS

Choice of Mutation To Disrupt the ^{6}F1−^{2}F2 Interface. To investigate the role of the ^{6}F1−^{2}F2 interaction, a residue within the hydrophobic interface was mutated in order to disrupt it (Figure 1). The small nonpolar residue A114 in the ^{2}F2 module was chosen as the site for mutation as several intermodule NOEs were observed from this side chain to residues in the ^{6}F1 module in the structure determination of ^{6}F1^{1}F2^{2}F2 (*20*). Mutating this residue is unlikely to disrupt

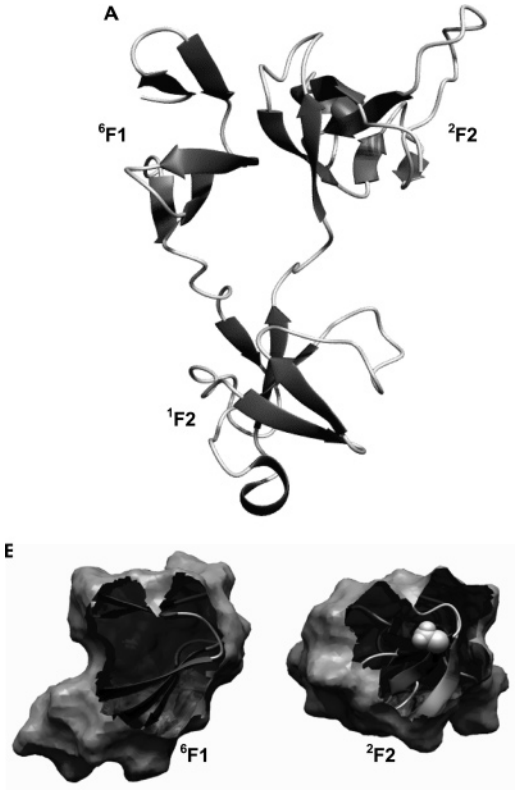

FIGURE 1: Selection of the target residue for mutagenesis. (A) Ribbon diagram of the ^{6}F1^{1}F2^{2}F2 fragment showing the hairpin topology (*20*). (B) An "exploded" view of the ^{6}F1−^{2}F2 intermodule interface. The ribbon diagrams of ^{6}F1 and ^{2}F2 are shown surrounded by their solvent-accessible surfaces. The two modules have been rotated outward by 90° to show the solvent inaccessibility of the A114 side chain in the intermodule interface. These molecular models and those in Figure 4 were generated with the programs MOLMOL (*28*) and POV-Ray (http://www.povray.org).

the basic fold of the ^{2}F2 module because A114 lies in a nonconserved position in the F2 module consensus sequence (*25*). Thus, A114 was mutated to aspartate (A114D) in the hope that the introduction of the negative charge would prevent the ^{6}F1 and ^{2}F2 modules from annealing together. This mutation was incorporated into both ^{6}F1^{1}F2^{2}F2 and ^{1}F2^{2}F2 so that its effect on the structure and function of the ^{2}F2 module per se could be evaluated.

Structural Characterization of the A114D Mutant. NMR spectral assignment of the A114D mutants was conducted by comparison of HSQC spectra with their wild-type counterparts and confirmed by 3D HSQC-TOCSY and NOESY experiments. The ^{1}F2^{2}F2(A114D) residues T101, S111, N112, G155, and F156 showed significant chemical shift differences from the wild-type ^{1}F2^{2}F2. These local changes in chemical shift reflect the introduction of a negative charge at A114D. The restricted distribution of these chemical shift changes implies, however, that the mutation does not significantly affect the intrinsic structure of the ^{2}F2 module.

The ^{6}F1−^{2}F2 intermodule interface in wild-type ^{6}F1^{1}F2-^{2}F2 can be readily detected by comparison of the NMR chemical shifts of overlapping fragments under identical solution conditions (*20*). Long-range changes in chemical shift of the ^{2}F2 resonances were seen upon removal of the ^{6}F1 module and of ^{6}F1 resonances on removal of the ^{2}F2 module. No such long-range chemical shift changes were

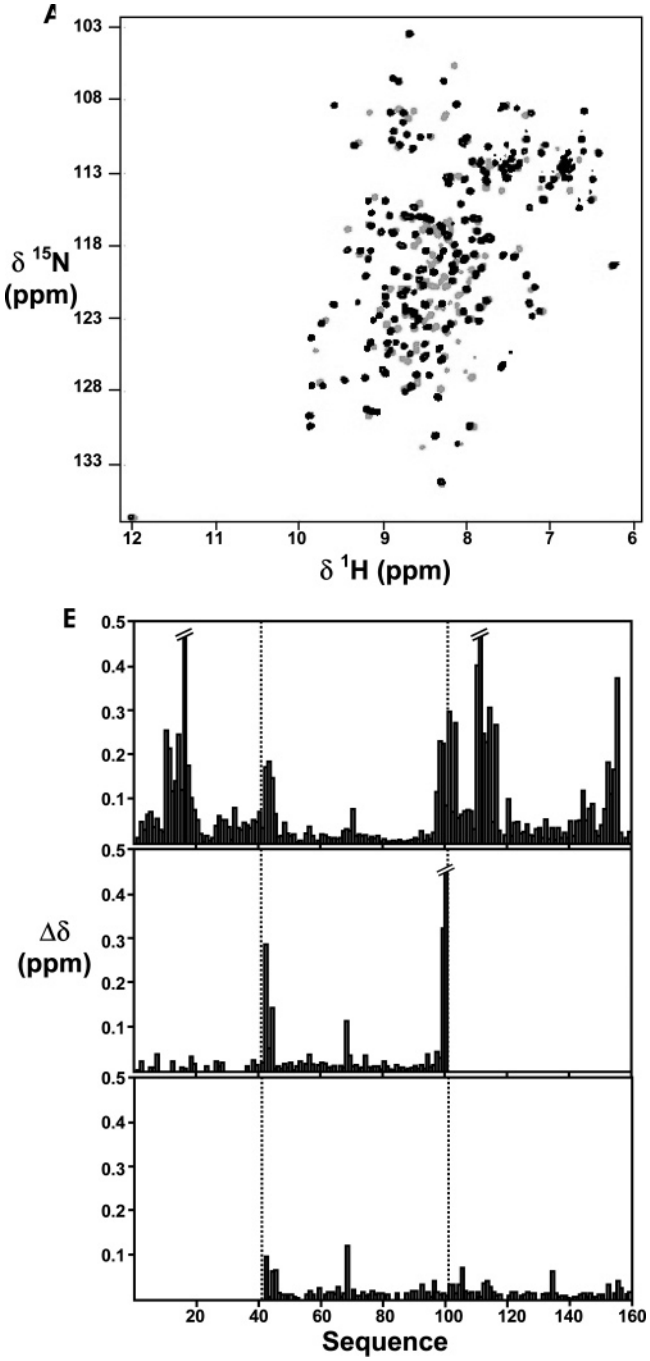

FIGURE 2: Structural perturbation caused by the A114D mutation. (A) Overlaid HSQC spectra of wild-type ^{6}F1^{1}F2^{2}F2 (black) and ^{6}F1^{1}F2^{2}F2(A114D) (gray). (B) Combined amide chemical shift differences ($\Delta\delta$) of the amide proton (H^N) and amide nitrogen (N^H) backbone resonances between ^{6}F1^{1}F2^{2}F2 and ^{6}F1^{1}F2^{2}F2(A114D) (top), ^{6}F1^{1}F2 and ^{6}F1^{1}F2^{2}F2(A114D) (middle), and ^{1}F2^{2}F2(A114D) and ^{6}F1^{1}F2^{2}F2(A114D) (bottom). In each panel, the vertical dotted lines mark the exon boundaries between the modules, and $\Delta\delta = \{|\Delta H^N| + (|\Delta N^H|/5)\}/2$, where Δ is the chemical shift difference.

observed for the ^{6}F1^{1}F2^{2}F2(A114D) mutant, and removal of ^{6}F1 had essentially no effect on ^{2}F2 resonance positions. Similarly, removal of ^{2}F2 had no effect on ^{6}F1 resonances (Figure 2). Comparison of ^{6}F1^{1}F2^{2}F2(A114D) spectra with wild-type ^{6}F1^{1}F2^{2}F2 spectra (Figure 2) shows chemical shift changes in both the ^{6}F1 and ^{2}F2 modules, as would be expected if the ^{6}F1−^{1}F2 interface were no longer present in the A114D mutant. Both of these lines of evidence can be interpreted in terms of the A114D mutation destabilizing and

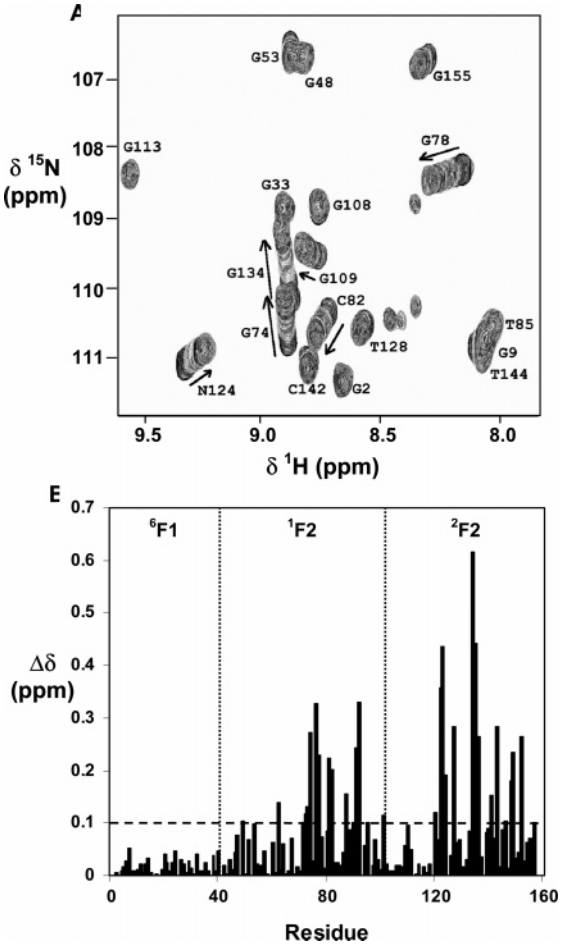

FIGURE 3: Ligand dependence of the ^{6}F1^{1}F2^{2}F2 chemical shifts. (A) Changes in ^{1}H,^{15}N-HSQC spectra produced by addition of the gelatin-like peptide GPAGAOGTOGPQGIAG to [u-^{15}N]^{6}F1^{1}F2-^{2}F2 at pH 4.5. (B) Amide chemical shift change ($\Delta\delta$) at a peptide:protein ratio of 5:1, where $\Delta\delta$ is as defined in Figure 2. The vertical dotted lines mark the exon boundaries between the modules, and the horizontal dashed line at 0.1 ppm marks the significance cutoff. Those titrating resonances which were perturbed by more than this value were used in the derivation of the affinity constants.

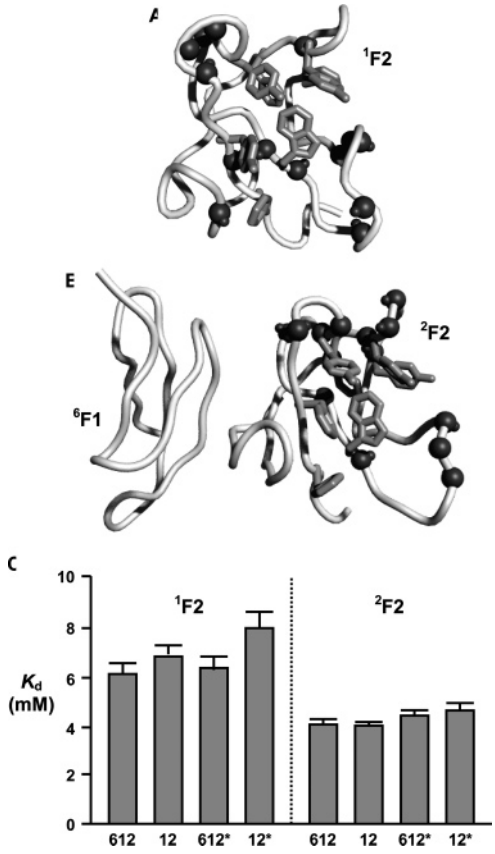

FIGURE 4: Gelatin binding sites in the ^{6}F1^{1}F2^{2}F2 fragment. The binding sites of (A) the ^{1}F2 module and (B) the ^{2}F2 module are shown. The cluster of aromatic side chains that partly constitute the binding sites is shown in light gray, and those amide groups that show significant chemical shift changes upon titration with the gelatin peptide are shown in dark gray. (C) Calculated dissociation constants for a two-site binding model to the F2 modules of each fragment. The error bars show the standard deviation in best-fit K_d following the addition of random Gaussian errors to the measured chemical shifts. Small discrepancies in peptide concentration also contribute to the errors in this experiment and the determination of K_d values.

disrupting the ^{6}F1−^{2}F2 interface that is present in the wild-type protein.

NMR-Monitored Gelatin Peptide Binding. The effect of the A114D mutation on the gelatin binding activity of the individual modules was assessed using NMR-monitored peptide titrations. In each case, chemical shift changes were in the fast exchange regime (Figure 3A) and were limited to the ^{1}F2 and ^{2}F2 modules; no significant chemical shift perturbations were observed in the ^{6}F1 (Figure 3B). In each F2 module, the backbone amide resonances most affected are found in regions surrounding the cluster of solvent-exposed aromatic residues (Figure 4A,B). These F2 module surfaces were previously predicted to form the collagen binding sites (*25*, *26*).

Since a preliminary modeling study suggested that the peptide was too short to bridge the gelatin binding sites on the two F2 modules (data not shown), the data were initially fit to a model of two noncooperative binding sites. The gelatin peptide dissociation constants determined from the Monte Carlo optimization of K_d and $\Delta_{\infty}^{r,s}$ are shown in Figure 4C. In each protein, the ^{2}F2 module binds with higher affinity than the ^{1}F2 module, thus validating the noncooperative model assumption. By comparison of the K_d values of ^{1}F2^{2}F2 with ^{1}F2^{2}F2(A114D) it can be seen that the gelatin binding activity of the ^{2}F2 module is largely unaffected by the A114D mutation. Furthermore, since the K_d values are identical for ^{6}F1^{1}F2^{2}F2 with ^{6}F1^{1}F2^{2}F2(A114D), the ^{6}F1−^{2}F2 intermodule interface has essentially no effect on each F2 module's intrinsic gelatin binding activity.

Gelatin Affinity Chromatography. To assess the possible influence of the ^{6}F1−^{2}F2 interface on the cooperation between fibronectin modules in binding to ligand, the fragments were analyzed using analytical gelatin affinity chromatography. This system has already been used successfully to monitor the affinity of a variety of fibronectin fragments (*19*). This method was also found to be more reliable than surface plasmon resonance because of difficulties in reproducibly immobilizing collagen/gelatin surfaces. In line with previous studies (*19*), the ^{6}F1^{1}F2^{2}F2 fragment was found to interact only transiently with the gelatin affinity column and was therefore eluted isocratically over time. This is in contrast to the intact gelatin binding domain of fibronectin which, in our hands (data not shown) and in others (*19*), requires the addition of 3−4 M urea for elution from the affinity column. This is testament to the contributing

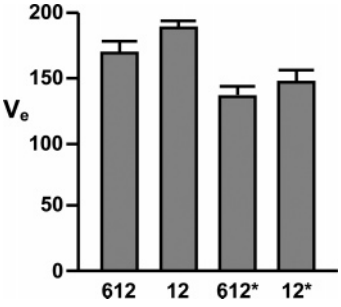

FIGURE 5: Average retardation and standard deviation (taken from three separate experiments) of various fragments of the gelatin binding domain (as marked) on a gelatin affinity column loaded with 100 μL of 8 μM wild-type ^{6}F1^{1}F2^{2}F2 (612), wild-type ^{1}F2-^{2}F2 (12), ^{6}F11F12^{2}F2(A114D) (612*), and ^{1}F2^{2}F2(A114D) (12*).

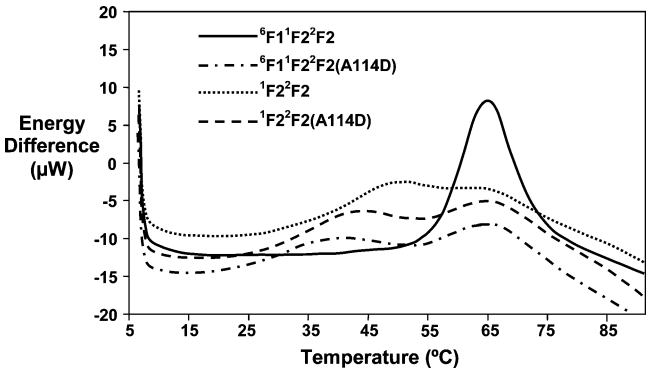

FIGURE 6: Differential scanning calorimetry plots for wild-type ^{6}F1^{1}F2^{2}F2, the ^{6}F1^{1}F2^{2}F2(A114D) mutant, wild-type ^{1}F2^{2}F2, and the ^{1}F2^{2}F2(A114D) mutant.

role of the ^{7}F1, ^{8}F1, and ^{9}F1 modules, each of which possesses gelatin binding activity (*17*, *19*, *27*).

As shown in Figure 5, the gelatin affinity column retards the ^{1}F2^{2}F2 and^{1}F2^{2}F2(A114D) module pairs more than ^{6}F1-^{1}F2^{2}F2 and ^{6}F1^{1}F2^{2}F2(A114D), respectively. This suggests that addition of the ^{6}F1 module reduces the gelatin binding affinity of both ^{1}F2^{2}F2 pairs. This reduction in the binding of fragments of the gelatin binding domain caused by addition of ^{6}F1 has also been observed by others (*19*). The ^{6}F1^{1}F2^{2}F2 wild-type fragment is retarded more than the ^{6}F1^{1}F2^{2}F2(A114D) mutant. However, the difference in elution volumes is the same as that between ^{1}F2^{2}F2 and ^{1}F2-^{2}F2(A114D), suggesting that it is the A114D mutation itself rather than disruption of the ^{6}F1−^{2}F2 interface that alters the binding affinity of these three-module fragments. Thus the ^{6}F1−^{2}F2 interface appears to have no significant effect on the gelatin binding affinity of the ^{6}F1^{1}F2^{2}F2 fragment of fibronectin.

Module Stabilization by the ^{6}F2−^{2}F2 Interface. If the ^{6}F1−^{2}F2 interface is not involved in gelatin binding, could it be involved in the stabilization of the ^{2}F2 module? Instability of the A114D mutants compared to their wild-type counterparts was observed during the fermentation and subsequent purification of these mutants. This instability was further investigated using differential scanning calorimetry (DSC) on wild-type and mutant ^{6}F1^{1}F2^{2}F2 and ^{1}F2^{2}F2 fragments (Figure 6). Previous studies have shown that the ^{6}F1 module is stable, in normal buffer conditions, to repeated heating to over 90 °C (*17*).

Both ^{1}F2^{2}F2 and ^{1}F2^{2}F2(A114D) have two melting transitions (Figure 6), an upper melting transition at 65 °C and a lower melting transition at 50 °C (wild type) or 41 °C (mutant). Since the only difference between these proteins is the A114D mutation, it is reasonable to assign this lower temperature transition to the melting of the ^{2}F2 module, while the transition at 65 °C represents the melting of ^{1}F2. The A114D mutation has slightly destabilized the ^{2}F2 module, reducing its melting temperature by 9 °C.

The wild-type ^{6}F1^{1}F2^{2}F2 melts with a single higher energy transition at 65 °C corresponding to the simultaneous melting of both F2 modules (Figure 6). The 15 °C stabilization of the ^{2}F2 module relative to the wild-type ^{1}F2^{2}F2 module pair must result from the ^{6}F1−^{2}F2 intermodule interface. This stabilizing interaction is lost in ^{6}F1^{1}F2^{2}F2(A114D) where the ^{2}F2 module undergoes a melting transition at 44 °C.

DISCUSSION

This paper has shown that the extensive hydrophobic interface between the noncontiguous ^{6}F1 and ^{2}F2 modules in fibronectin can be disrupted by the ^{2}F2 point mutation A114D. This mutation does not significantly impair the intrinsic gelatin binding activity of the ^{2}F2 module. It is shown that, in the context of a three-module fragment of fibronectin, this interface has very little effect on binding affinity to collagen-derived peptides or a gelatin affinity column. The mutation does, however, have a significant impact on protein stability. The enhanced stability conferred by the ^{6}F1−^{2}F2 interaction could be advantageous to the protein in its physiological role.

The gelatin affinity results (Figure 5) are in complete agreement with the results of Katagiri et al., who showed that deletion of the ^{6}F1 module from either the ^{6}F1^{1}F2^{2}F2-^{7}F1^{8}F1 or ^{6}F1^{1}F2^{2}F2^{7}F1^{8}F1^{9}F1 fragments resulted in a pronounced increase in gelatin affinity (*19*). The authors argued that the ^{6}F1−^{2}F2 interface imposes a constraint on the structure of the gelatin binding domain that impairs gelatin binding (*19*). The data presented here show that the abolition of this interface by the A114D mutation relieves this structural constraint and allows the two F2 modules to adopt a more favorable conformation for binding to gelatin. There is some conflict with our own previous studies (*20*) on the wild-type ^{1}F2^{2}F2 and ^{6}F1^{1}F2^{2}F2 fragments, but these were obtained using surface plasmon resonance, which we have subsequently found to be unreliable for studying gelatin binding. In the present study, no significant chemical shift perturbations on the ^{6}F1 module were observed upon the addition of collagen-derived peptides, suggesting that there is no direct contact between this module and the gelatin ligand.

What, then, is the physiological role of the ^{6}F1 module? We believe that the ^{6}F1−^{2}F2 pairing may provide a structural nucleus around which other modules are arranged to form the fully active gelatin binding domain. Thus, this entity may provide interaction surfaces for the ^{7}F1 module [as predicted by Litvinovich et al. from thermodynamic studies (*17*)] or even for the ^{8}F1 and/or ^{9}F1 modules since, as shown in the solution structure of ^{6}F1^{1}F2^{2}F2, modules need not be contiguous for an intimate interaction to take place. Furthermore, a ligand recognition site that is contiguous in space does not necessarily have to span fibronectin modules that are linear in sequence. Further clarification of these issues requires the structural determination of larger fragments of

the gelatin binding domain and a mapping of its gelatin binding surfaces.

ACKNOWLEDGMENT

The authors thank Robin Aplin and Tony Willis for assistance with mass spectrometry and N-terminal sequencing, respectively.

REFERENCES

1. Chen, H., and Mosher, D. F. (1996) Formation of sodium dodecyl sulfate-stable fibronectin multimers, *J. Biol. Chem. 271*, 9084−9089.
2. Magnusson, M. K., and Mosher, D. F. (1998) Fibronectin. Structure, assembly, and cardiovascular implications, *Arterioscler., Thromb., Vasc. Biol. 18*, 1363−1370.
3. Schwarzbauer, J. E., and Sechler, J. L. (1999) Fibronectin fibrillogenesis: a paradigm for extracellular matrix assembly, *Curr. Opin. Cell Biol. 11*, 622−627.
4. Sottile, J., and Mosher, D. F. (1993) Assembly of fibronectin molecules with mutations or deletions of the carboxyl-terminal type I modules, *Biochemistry 32*, 1641−1647.
5. Mercurius, K. O., and Morla, A. O. (2001) Cell adhesion and signaling on the fibronectin 1st type III repeat; requisite roles for cell surface proteoglycans and integrins, *BMC Cell Biol. 2*, 18−30.
6. Armstrong, P. B., and Armstrong, M. T. (2000) Intercellular invasion and the organizational stability of tissues: a role for fibronectin, *Biochim. Biophys. Acta 1470*, O9−O20.
7. Johansson, S., Svineng, G., Wennerberg, K., Armulik, A., and Lohikangas, L. (1997) Fibronectin-integrin interactions, *Front. Biosci. 2*, d126−d146.
8. Danen, E. H. J., and Yamada, K. M. (2001) Fibronectin, integrins, and growth control, *J. Cell. Physiol. 189*, 1−13.
9. Engvall, E., Ruoslahti, E., and Miller, E. J. (1978) Affinity of fibronectin to collagens of different genetic types and to fibrinogen, *J. Exp. Med. 147*, 1584−1595.
10. Dessau, W., Sasse, J., Timpl, R., and von der Mark, K. (1978) Role of fibronectin and collagen types I and II in chondrocytic differentiation in vitro, *Ann. N.Y. Acad. Sci. 312*, 404−405.
11. Shimizu, M., Minakuchi, K., Moon, M., and Koga, J. (1997) Difference in interaction of fibronectin with type I collagen and type IV collagen, *Biochim. Biophys. Acta 1339*, 53−61.
12. Kleinman, H. K., McGoodwin, E. B., Martin, G. R., Klebe, R. J., Fietzek, P. P., and Woolley, D. E. (1978) Localization of the binding site for cell attachment in the alpha1(I) chain of collagen, *J. Biol. Chem. 253*, 5642−5646.
13. McDonald, J. A., Kelley, D. G., and Broekelmann, T. J. (1982) Role of fibronectin in collagen deposition: Fab′ to the gelatin-binding domain of fibronectin inhibits both fibronectin and collagen organization in fibroblast extracellular matrix, *J. Cell Biol. 92*, 485−492.
14. Ingham, K. C., Brew, S. A., and Isaacs, B. S. (1988) Interaction of fibronectin and its gelatin-binding domains with fluorescent-labeled chains of type I collagen, *J. Biol. Chem. 263*, 4624−4628.
15. Balian, G., Click, E. M., Crouch, E., Davidson, J. M., and Bornstein, P. (1979) Isolation of a collagen-binding fragment from fibronectin and cold-insoluble globulin, *J. Biol. Chem. 254*, 1429−1432.
16. Hahn, L.-H. E., and Yamada, K. M. (1979) Identification and isolation of a collagen-binding fragment of the adhesive glycoprotein fibronectin, *Proc. Natl. Acad. Sci. U.S.A. 76*, 1160−1163.
17. Litvinovich, S. V., Strickland, D. K., Medved, L. V., and Ingham, K. C. (1991) Domain structure and interactions of the type I and type II modules in the gelatin-binding region of fibronectin: All six modules are independently folded, *J. Mol. Biol. 217*, 563−575.
18. Bányai, L., and Patthy, L. (1991) Evidence for the involvement of type II domains in collagen binding by 72 kDa type IV procollagenase, *FEBS Lett. 282*, 23−25.
19. Katagiri, Y., Brew, S. A., and Ingham, K. C. (2003) All six modules of the gelatin-binding domain of fibronectin are required for full affinity, *J. Biol. Chem. 278*, 11897−11902.
20. Pickford, A. R., Smith, S. P., Staunton, D., Boyd, J., and Campbell, I. D. (2001) The hairpin structure of the ^{6}F1^{1}F2^{2}F2 fragment from human fibronectin enhances gelatin binding, *EMBO J. 20*, 1519−1529.
21. Bright, J. R., Pickford, A. R., Potts, J. R., and Campbell, I. D. (2000) Preparation of isotopically labeled recombinant fragments of fibronectin for functional and structural study by heteronuclear nuclear magnetic resonance spectroscopy, *Methods Mol. Biol. 139*, 59−69.
22. Marion, D., Driscoll, P. C., Kay, L. E., Wingfield, P. T., Bax, A., Gronenborn, A. M., and Clore, G. M. (1989) Overcoming the overlap problem in the assignment of proton NMR spectra of larger proteins by use of three-dimensional heteronuclear proton−nitrogen-15 Hartmann−Hahn-multiple quantum coherence and nuclear Overhauser-multiple quantum coherence spectroscopy: application to interleukin 1β, *Biochemistry 28*, 6150−6156.
23. Wishart, D. S., Bigam, C. G., Yao, J., Abilgaard, F., Dyson, H. J., Oldfield, E., Markley, J. L., and Sykes, B. D. (1995) ^{1}H, ^{13}C and ^{15}N chemical shift referencing in biomolecular NMR, *J. Biomol. NMR 6*, 135−140.
24. Bocquier, A. A., Potts, J. R., Pickford, A. R., and Campbell, I. D. (1999) Solution structure of a pair of modules from the gelatin-binding domain of fibronectin, *Struct. Folding Des. 7*, 1451−1460.
25. Pickford, A. R., Potts, J. R., Bright, J. R., Phan, I., and Campbell, I. D. (1997) Solution structure of a type 2 module from fibronectin: implications for the structure and function of the gelatin-binding domain, *Structure 5*, 359−370.
26. Sticht, H., Pickford, A. R., Potts, J. R., and Campbell, I. D. (1998) Solution structure of the glycosylated second type 2 module of fibronectin, *J. Mol. Biol. 276*, 177−187.
27. Millard, C. J., Campbell, I. D., and Pickford, A. R. (2005) Gelatin binding to the ^{8}F1^{9}F1 module pair of human fibronectin requires site-specific N-glycosylation, *FEBS Lett. 579*, 4529−4534.
28. Koradi, R., Billeter, M., and Wüthrich, K. (1996) MOLMOL: a program for display and analysis of macromolecular structures, *J. Mol. Graphics 14*, 51−55.
29. Potts, J. R., and Campbell, I. D. (1996) Structure and function of fibronectin modules, *Matrix Biol. 15*, 313−320.

BI050937I